Eur. Phys. J. B **27**, 303–311 (2002)
DOI: 10.1140/epjb/e2002-00159-0

THE EUROPEAN PHYSICAL JOURNAL B

Relation between vortex excitation and thermal conductivity in superconductors

M. Takigawa[a], M. Ichioka, and K. Machida

Department of Physics, Okayama University, Okayama 700-8530, Japan

Received 8 December 2001 and Received in final form 20 March 2002
Published online 6 June 2002 –

Abstract. Thermal conductivity $\kappa_{xx}(T)$ under a field is investigated in $d_{x^2-y^2}$-wave superconductors and isotropic s-wave superconductors by the linear response theory, using a microscopic wave function of the vortex lattice states. To study the origin of the different field dependence of $\kappa_{xx}(T)$ between higher and lower temperature regions, we analyze the spatially-resolved thermal conductivity around a vortex at each temperature, which is related to the spectrum of the local density of states. We also discuss the electric conductivity in the same formulation for a comparison.

PACS. 74.60.Ec Mixed state – 74.25.Fy Transport properties – 74.25.Jb Electronic structure

1 Introduction

Recent advance to synthesize new exotic superconducting materials further requires the experimental probes to precisely identify their pairing functions consisting of the orbital and spin components. The orbital part of the pairing function determines the nodal structure of the energy gap on the Fermi surface. Thermal conductivity is one of the standard techniques to probe the node of the gap structure [1–6]. One can basically extract the gap topology such as line or point nodes by analyzing its dependence on the temperature T.

In the vortex state under a magnetic field, the thermal conductivity is affected by the low energy quasiparticle state around the vortex [6–8]. So far, the thermal conductivity in the vortex state has been investigated by the theory of gapless superconductors at high field [9,10], or the theory considering vortices as scattering centers [11], and estimating the electron-vortex scattering rate [12–14]. Recently, the thermal conductivity in the vortex state of high-T_c superconductors attracts much attention, because the quasiparticle states are qualitatively different in the vortex state between the d-wave pairing case and the conventional s-wave pairing case. In the s-wave pairing, low energy quasiparticle states are bound around the vortex core [15,16]. In the d-wave pairing, low energy quasiparticle states around the vortex extend outside of the vortex core due to the line node of the superconducting gap [17–22]. The contribution to the thermal conductivity from the quasiparticles outside of the core is investigated by the theory of the Doppler shift (or the Dirac fermion) in the d-wave pairing case [23–25]. Since these theory neglect the contribution from the quasiparticle within the vortex core [17], they are not applied to the s-wave superconductors.

Here, we calculate the T-dependence of the thermal conductivity under a field. Our calculation is based on a microscopic theory of Bogoliubov-de Gennes (BdG) equation for describing the vortex state [26–28] and standard linear response theory for the thermal conductivity [29,30], assuming a clean-limit type II superconductors. Our calculation includes all contributions from the inside and the outside region of the vortex core. The spatial distribution of the thermal conductivity is calculated from the wave function of the vortex lattice state, and analyzed by compared with the spatial distribution of the local density of states (LDOS).

The rest of this paper is organized as follows. In Section 2, we describe our formulation based on the BdG equation and the linear response theory. In Section 3, we study the dependence of the thermal conductivity on the temperature in the vortex state. We also show the position-resolved thermal conductivity and its energy decomposition, and discuss the relation with the LDOS. In Section 4, we investigate the electric conductivity in the same formulation, and discuss the difference of the quasiparticle contribution between the thermal conductivity and electric conductivity. The summary and discussions are given in Section 5.

2 Formulation

2.1 Bogoliubov-de Gennes equation

We obtain the wave function in the vortex lattice state by solving the BdG equation for the extended Hubbard model [26–28] defined on a two dimensional square lattice.

[a] e-mail: takigawa@mp.okayama-u.ac.jp

From this model, we obtain qualitatively the same quasiparticle structure as previous theoretical studies both for the s-wave [15,16] case and for the d-wave [17–22] case. Here we briefly discuss the BdG equation for the s-wave pairing and the d-wave pairing cases, which is written as

$$\sum_j \begin{pmatrix} K_{i,j} & D_{i,j} \\ D_{i,j}^\dagger & -K_{i,j}^* \end{pmatrix} \begin{pmatrix} u_\alpha(\mathbf{r}_j) \\ v_\alpha(\mathbf{r}_j) \end{pmatrix} = E_\alpha \begin{pmatrix} u_\alpha(\mathbf{r}_i) \\ v_\alpha(\mathbf{r}_i) \end{pmatrix}, \quad (1)$$

where

$$K_{i,j} = -\tilde{t}_{i,j} - \delta_{i,j}\mu, \quad (2)$$

$$\tilde{t}_{i,j} = t_{i,j} \exp\left[\mathrm{i}\frac{\pi}{\phi_0}\int_{\mathbf{r}_i}^{\mathbf{r}_j} \mathbf{A}(\mathbf{r})\cdot \mathrm{d}\mathbf{r}\right], \quad (3)$$

$$D_{i,j} = \delta_{i,j} U \Delta_{i,i} + \frac{1}{2} V_{i,j} \Delta_{i,j} \quad (4)$$

with the on-site interaction U, the flux quantum ϕ_0 and the chemical potential μ. The nearest neighbor (NN) transfer integral $t_{i,j} = t$ and the NN interaction $V_{i,j} = V$ for the NN site pair $\mathbf{r}_i$ and $\mathbf{r}_{i\pm\hat{e}}$. The vector potential $\mathbf{A}(\mathbf{r}) = \frac{1}{2}\mathbf{H}\times\mathbf{r}$ in the symmetric gauge. Since we assume an extreme type-II superconductor, the internal field term of $\mathbf{A}(\mathbf{r})$ is neglected. The self-consistent condition for the pair potential is

$$\Delta_{i,j} = -\frac{1}{2}\sum_\alpha u_\alpha(\mathbf{r}_i) v_\alpha^*(\mathbf{r}_j) \tanh(E_\alpha/2T). \quad (5)$$

The s-wave pair potential is given by

$$\Delta_s(\mathbf{r}_i) = U\Delta_{i,i}. \quad (6)$$

The $d_{x^2-y^2}$-wave pair potential is

$$\Delta_d(\mathbf{r}_i) = \frac{V}{4}(\Delta_{\hat{x},i} + \Delta_{-\hat{x},i} - \Delta_{\hat{y},i} - \Delta_{-\hat{y},i}) \quad (7)$$

with

$$\Delta_{\pm\hat{e},i} = \Delta_{i,i\pm\hat{e}} \exp\left[\mathrm{i}\frac{\pi}{\phi_0}\int_{\mathbf{r}_i}^{(\mathbf{r}_i+\mathbf{r}_{i\pm\hat{e}})/2} \mathbf{A}(\mathbf{r})\cdot\mathrm{d}\mathbf{r}\right]\cdot \quad (8)$$

We study the case of the square vortex lattice where the NN vortex is located in the direction of 45° from the a-axis. This vortex lattice configuration is suggested for d-wave superconductors and s-wave superconductors with fourfold symmetric Fermi surface [20,31–34]. The unit cell in our calculation is the square area of ${N_r}^2$ sites where two vortices are accommodated. Then, $H = 2\phi_0/(aN_r)^2$ with the lattice constant a. Thus, we denote the field strength by N_r as H_{N_r}. Since H should be commensurate with the atomic lattice, our formulation does not treat the field dependence continuously. We consider the area of ${N_k}^2$ unit cells. By introducing the quasi-momentum of the magnetic Bloch state, $\mathbf{k} = (2\pi/aN_rN_k)(l_x,l_y)$:$(l_x,l_y = 1,2,\cdots,N_k)$, we set $u_\alpha(\mathbf{r}) = \tilde{u}_\alpha(\mathbf{r})\mathrm{e}^{\mathrm{i}\mathbf{k}\cdot\mathbf{r}}, v_\alpha(\mathbf{r}) = \tilde{v}_\alpha(\mathbf{r})\mathrm{e}^{\mathrm{i}\mathbf{k}\cdot\mathbf{r}}$. Then, the eigenstate of α is labeled by $\mathbf{k}$ and the eigenvalues obtained by this calculation within a unit cell.

The periodic boundary condition is given by the symmetry for the translation $\mathbf{R} = l_x\mathbf{R}_x^0 + l_y\mathbf{R}_y^0$, where $\mathbf{R}_x^0 = (aN_r,0)$ and $\mathbf{R}_y^0 = (0,aN_r)$ are unit vectors of the unit cell for our calculation. Then, the translational relation is given by $\tilde{u}_\alpha(\mathbf{r}+\mathbf{R}) = \tilde{u}_\alpha(\mathbf{r})\mathrm{e}^{\mathrm{i}\chi(\mathbf{r},\mathbf{R})/2}, \tilde{v}_\alpha(\mathbf{r}+\mathbf{R}) = \tilde{v}_\alpha(\mathbf{r})\mathrm{e}^{-\mathrm{i}\chi(\mathbf{r},\mathbf{R})/2}$. Here,

$$\chi(\mathbf{r},\mathbf{R}) = -\frac{2\pi}{\phi_0}\mathbf{A}(\mathbf{R})\cdot\mathbf{r} - 2\pi l_x(l_x-l_y) + \frac{2\pi}{\phi_0}(\mathbf{H}\times\mathbf{r}_0)\cdot\mathbf{R} \quad (9)$$

in the symmetric gauge. The vortex center is located at $\mathbf{r}_0 + \frac{1}{4}(3\mathbf{R}_x^0 + \mathbf{R}_y^0)$. The phase factor in equation (8) is necessary to satisfy the translational relation $\Delta_d(\mathbf{r}+\mathbf{R}) = \Delta_d(\mathbf{r})\mathrm{e}^{\mathrm{i}\chi(\mathbf{r},\mathbf{R})}$.

The following parameter values are chosen in the calculation. The average electron density per site ~ 0.9 by appropriately adjusting the chemical potential μ. We normalize all the energy scales by the transfer integral t. For the s-wave case, we set $U = -2.32t$ and $V = 0$. The resulting order parameter $\Delta_0 = 0.5t$ at $T = H = 0$, and the superconducting transition temperature $T_c \sim 0.27t$. For the d-wave case, we set $U = 0$ and $V = -4.2t$. Then, $\Delta_0 = 1.0t$, and $T_c \sim 0.42t$. Our results do not qualitatively depend on the choice of these parameters.

2.2 Local density of states

In order to calculate physical quantities, we must construct the Green's functions from E_α,$u_\alpha(\mathbf{r})$,$v_\alpha(\mathbf{r})$ in the formulation of imaginary time τ and Fermionic Matsubara frequency $\omega_n = 2\pi T(n+\frac{1}{2})$. The Matsubara Green's functions is given by

$$\hat{g}(\mathbf{r},\mathbf{r}',\mathrm{i}\omega_n) = \begin{pmatrix} g_{11}(\mathbf{r},\mathbf{r}',\mathrm{i}\omega_n) & g_{12}(\mathbf{r},\mathbf{r}',\mathrm{i}\omega_n) \\ g_{21}(\mathbf{r},\mathbf{r}',\mathrm{i}\omega_n) & g_{22}(\mathbf{r},\mathbf{r}',\mathrm{i}\omega_n) \end{pmatrix}, \quad (10)$$

where matrix components are Fourier transformation of

$$g_{11}(\mathbf{r},\tau,\mathbf{r}',\tau') = -\left\langle T_\tau[\psi_\uparrow(\mathbf{r},\tau)\psi_\uparrow^\dagger(\mathbf{r}',\tau')]\right\rangle, \quad (11)$$

$$g_{12}(\mathbf{r},\tau,\mathbf{r}',\tau') = -\left\langle T_\tau[\psi_\uparrow(\mathbf{r},\tau)\psi_\downarrow(\mathbf{r}',\tau')]\right\rangle, \quad (12)$$

$$g_{21}(\mathbf{r},\tau,\mathbf{r}',\tau') = -\left\langle T_\tau[\psi_\downarrow^\dagger(\mathbf{r},\tau)\psi_\uparrow^\dagger(\mathbf{r}',\tau')]\right\rangle, \quad (13)$$

$$g_{22}(\mathbf{r},\tau,\mathbf{r}',\tau') = -\left\langle T_\tau[\psi_\downarrow^\dagger(\mathbf{r},\tau)\psi_\downarrow(\mathbf{r}',\tau')]\right\rangle\cdot \quad (14)$$

The Green's functions in equation (10) as follows [28],

$$g_{11}(\mathbf{r},\mathbf{r}',\mathrm{i}\omega_n) = \sum_\alpha \frac{u_\alpha(\mathbf{r})u_\alpha^*(\mathbf{r}')}{\mathrm{i}\omega_n - E_\alpha}, \quad (15)$$

$$g_{12}(\mathbf{r},\mathbf{r}',\mathrm{i}\omega_n) = \sum_\alpha \frac{u_\alpha(\mathbf{r})v_\alpha^*(\mathbf{r}')}{\mathrm{i}\omega_n - E_\alpha}, \quad (16)$$

$$g_{21}(\mathbf{r},\mathbf{r}',\mathrm{i}\omega_n) = \sum_\alpha \frac{v_\alpha(\mathbf{r})u_\alpha^*(\mathbf{r}')}{\mathrm{i}\omega_n - E_\alpha}, \quad (17)$$

$$g_{22}(\mathbf{r},\mathbf{r}',\mathrm{i}\omega_n) = \sum_\alpha \frac{v_\alpha(\mathbf{r})v_\alpha^*(\mathbf{r}')}{\mathrm{i}\omega_n - E_\alpha}\cdot \quad (18)$$

The LDOS is given by the thermal Green's functions as

$$N_\uparrow(E,\mathbf{r}) = -\frac{1}{\pi}\mathrm{Im}g_{11}(\mathbf{r},\mathbf{r},\mathrm{i}\omega_n \to E+\mathrm{i}0^+) = \sum_\alpha |u_\alpha(\mathbf{r})|^2\delta(E-E_\alpha) \quad (19)$$

for the up-spin electron contributions, and

$$N_\downarrow(E,\mathbf{r}) = \frac{1}{\pi}\mathrm{Im}g_{22}(\mathbf{r},\mathbf{r},-\mathrm{i}\omega_n \to E+\mathrm{i}0^+) = \sum_\alpha |v_\alpha(\mathbf{r})|^2\delta(E+E_\alpha) \quad (20)$$

for the down-spin electron contributions. Therefore, the LDOS is given by

$$N(E,\mathbf{r}) = N_\uparrow(E,\mathbf{r}) + N_\downarrow(E,\mathbf{r}) = \sum_\alpha \left\{|u_\alpha(\mathbf{r})|^2\delta(E-E_\alpha) + |v_\alpha(\mathbf{r})|^2\delta(E+E_\alpha)\right\}\cdot \quad (21)$$

2.3 Linear response theory

We calculate the thermal conductivity following the method of references [29] and [30]. According to the linear response theory, thermal current $h_x(\mathbf{r}_1)$ flowing to the x-direction at $\mathbf{r}_1$-site is given by

$$h_x(\mathbf{r}_1) = \frac{1}{T}\sum_{\mathbf{r}_2}\mathrm{Re}\left\{\frac{1}{\mathrm{i}}\frac{\mathrm{d}}{\mathrm{d}\Omega}Q_{xx}(\mathbf{r}_1,\mathbf{r}_2,\mathrm{i}\Omega_n \to \Omega+\mathrm{i}0^+)\right\}_{\Omega\to 0} \times(-\nabla_x T(\mathbf{r}_2)), \quad (22)$$

when the small temperature gradient $-\nabla_x T(\mathbf{r}_2)$ along the x-direction is applied at $\mathbf{r}_2$-site. The heat-heat correlation function is defined by

$$Q_{xx}(\mathbf{r}_1\tau_1,\mathbf{r}_2\tau_2) = \langle T_\tau[h_x(\mathbf{r}_1\tau_1),h_x(\mathbf{r}_2\tau_2)]\rangle = T\sum_n \mathrm{e}^{-\mathrm{i}\Omega_n(\tau_1-\tau_2)}Q_{xx}(\mathbf{r}_1,\mathbf{r}_2,\mathrm{i}\Omega_n) \quad (23)$$

in the formulation of imaginary time τ and Matsubara frequency Ω_n. The heat current operator $\mathbf{h}(\mathbf{r}_j,\tau)$ is written as

$$\mathbf{h}(\mathbf{r}_j,\tau) = -\frac{\mathrm{i}}{2m}\left(\mathbf{P}_j\frac{\partial}{\partial\tau'} - \mathbf{P}^\dagger_{j'}\frac{\partial}{\partial\tau}\right) \times\sum_\sigma \psi^\dagger_\sigma(\mathbf{r}_{j'},\tau')\psi_\sigma(\mathbf{r}_j,\tau)|_{j=j',\tau=\tau'} \quad (24)$$

in terms of the electron field operators $\psi_\sigma(\mathbf{r}_j,\tau)$. The x-component of the momentum operator $\mathbf{P}_j$ in the discretized square lattice is defined as

$$[\mathbf{P}_j\psi_\sigma(\mathbf{r}_j,\tau)]_x = \mathbf{a}\frac{2mt}{\mathrm{i}}\mathrm{e}^{\mathrm{i}(\pi/\phi_0)\mathbf{a}\cdot\mathbf{A}(\mathbf{r}_j+\mathbf{a}/2)}\psi_\sigma(\mathbf{r}_j+\mathbf{a},\tau) \quad (25)$$

with $\mathbf{a} = (a,0)$. Four electron field operators in equation (23) are decomposed by using the Matsubara Green's functions in equations (15–18) .

For the study of the thermal conductivity, we have to introduce the dissipation term η in the Green's function. Then, the retarded and advanced Green's functions are, respectively, given by $\hat{G}^{\mathrm{R}}(\mathbf{r},\mathbf{r}',\omega) = \hat{g}(\mathbf{r},\mathbf{r}',\mathrm{i}\omega_n \to \omega+\mathrm{i}\eta)$ and $\hat{G}^{\mathrm{A}}(\mathbf{r},\mathbf{r}',\omega) = \hat{g}(\mathbf{r},\mathbf{r}',\mathrm{i}\omega_n \to \omega-\mathrm{i}\eta)$. Therefore, in the spectral representation, we obtain

$$\hat{g}(\mathbf{r},\mathbf{r}',\mathrm{i}\omega_n) = \int_{-\infty}^{\infty}\frac{\mathrm{d}\omega}{2\pi}\frac{\hat{A}(\mathbf{r},\mathbf{r}',\omega)}{\mathrm{i}\omega_n-\omega}, \quad (26)$$

where

$$\hat{A}(\mathbf{r},\mathbf{r}',\omega) = -\frac{1}{2\pi\mathrm{i}}\left(\hat{G}^{\mathrm{R}}(\mathbf{r},\mathbf{r}',\omega) - \hat{G}^{\mathrm{A}}(\mathbf{r},\mathbf{r}',\omega)\right) = \sum_\alpha \delta_\eta(\omega-E_\alpha)\begin{pmatrix} u_\alpha(\mathbf{r})u^*_\alpha(\mathbf{r}') & u_\alpha(\mathbf{r})v^*_\alpha(\mathbf{r}') \\ v_\alpha(\mathbf{r})u^*_\alpha(\mathbf{r}') & v_\alpha(\mathbf{r})v^*_\alpha(\mathbf{r}')\end{pmatrix} \quad (27)$$

with $\delta_\eta(\omega) = \eta[\pi(\omega^2+\eta^2)]^{-1}$.

As a result, the heat-heat correlation function is reduced to

$$\begin{aligned}\frac{\mathrm{d}}{\mathrm{d}\Omega}Q_{\mathbf{P}_1\mathbf{P}_2}(\mathbf{r}_1,\mathbf{r}_2,\mathrm{i}\Omega_n \to \Omega+\mathrm{i}0^+)\Big|_{\Omega=0} = & \\ \frac{1}{4m^2}\sum_{\alpha\beta}F(E_\alpha,E_\beta) & \\ \times[\mathbf{P}_1 u_\alpha(\mathbf{r}_1)u^*_\beta(\mathbf{r}_{1'}) + u_\alpha(\mathbf{r}_1)\mathbf{P}^\dagger_{1'}u^*_\beta(\mathbf{r}_{1'}) & \\ +\mathbf{P}^\dagger_1 v_\alpha(\mathbf{r}_1)v^*_\beta(\mathbf{r}_{1'}) + v_\alpha(\mathbf{r}_1)\mathbf{P}_{1'}v^*_\beta(\mathbf{r}_{1'})] & \\ \times[\mathbf{P}_2 u_\alpha(\mathbf{r}_2)u^*_\beta(\mathbf{r}_{2'}) + u_\alpha(\mathbf{r}_2)\mathbf{P}^\dagger_{2'}u^*_\beta(\mathbf{r}_{2'}) & \\ +\mathbf{P}^\dagger_2 v_\alpha(\mathbf{r}_2)v^*_\beta(\mathbf{r}_{2'}) + v_\alpha(\mathbf{r}_2)\mathbf{P}_{2'}v^*_\beta(\mathbf{r}_{2'})]|_{1=1',2=2'}, & \quad (28)\end{aligned}$$

where

$$F(E_\alpha,E_\beta) = \int\frac{\mathrm{d}\omega}{2\pi}\int\frac{\mathrm{d}\omega'}{2\pi}\delta_\eta(\omega-E_\alpha)\delta_\eta(\omega'-E_\beta) \times\left[\mathrm{P}\frac{\omega^2 f(\omega)-\omega'^2 f(\omega')}{(\omega-\omega')^2} + \mathrm{i}\pi\omega^2 f'(\omega)\delta(\omega-\omega')\right]. \quad (29)$$

When the temperature gradient $\nabla_x T(\mathbf{r}_2)$ is uniform, the position-resolved thermal conductivity is written as

$$\kappa_{xx}(\mathbf{r}_1) = \frac{h_x(\mathbf{r}_1)}{-\nabla_x T} = \frac{1}{T}\mathrm{Im}\left\{\frac{\mathrm{d}}{\mathrm{d}\Omega}\frac{1}{N}\sum_{\mathbf{r}_2}Q_{xx}(\mathbf{r}_1,\mathbf{r}_2,\mathrm{i}\Omega_n \to \Omega+\mathrm{i}0^+)\right\}\cdot \quad (30)$$

The spatially averaged thermal conductivity

$$\kappa_{xx} = \frac{1}{N}\sum_{\mathbf{r}_1}\kappa_{xx}(\mathbf{r}_1) \quad (31)$$

is observed in the experiment. N is the total number of sites. At zero field, our formulation for κ_{xx} is reduced to

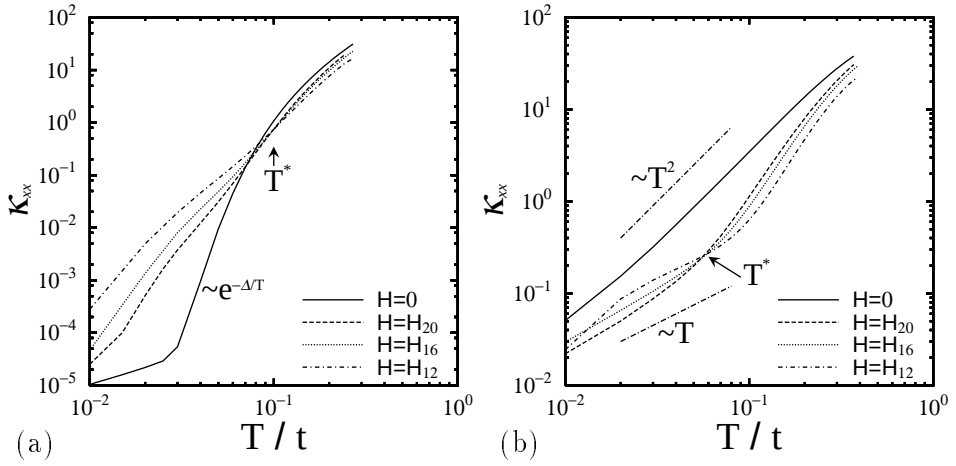

Fig. 1. Temperature dependence of $\kappa_{xx}(T)$ at $H = 0$, H_{20}, H_{16} and H_{12}. (a) s-wave case. (b) d-wave case.

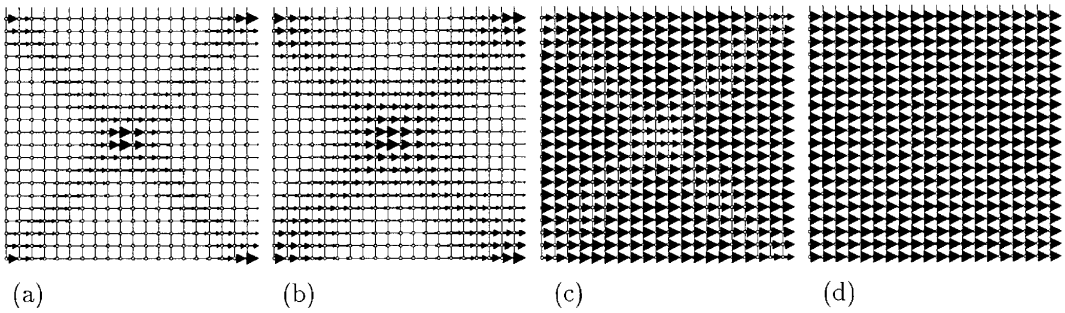

Fig. 2. The vector plots of the $\kappa_{xx}(\mathbf{r})$ in the s-wave pairing case at T/t=0.02 (a), 0.05 (b), 0.09 (c) and 0.13 (d). $H = H_{20}$. The vortices are located at the center and the four corners in the figure. Arrow size is proportional to flow strength.

the well-known formula for the uniform superconductors in the presence of impurity scattering [29].

Using the wave function $u_\alpha(\mathbf{r})$, $v_\alpha(\mathbf{r})$ and the eigenenergy E_α in equation (1), we calculate the dependence of κ_{xx} on the temperature and the field. And to analyze this behavior, we also study the spatial structure of $\kappa_{xx}(\mathbf{r})$, *i.e.*, the local contribution to κ_{xx}, Here, we neglect the principal value integral term $\mathrm{Re}F(E_\alpha, E_\beta)$ in equation (29), because the contribution from this term vanishes in the spatial average of $\kappa_{xx}(\mathbf{r})$. We typically choose $\eta = 0.01t$.

3 Thermal conductivity

3.1 Temperature dependence of thermal conductivity

The T-dependence of $\kappa_{xx}(T)$ is shown in Figures 1a and b for the s-wave and the d-wave pairing cases, respectively. For the s-wave pairing, it shows exponential T-dependence due to the full gap of the s-wave superconductivity at $H = 0$. It changes into a T-linear behavior at low T region in the vortex state at $H \neq 0$, reflecting low energy quasiparticle state around the vortex. We see also that the deviation from the expected T dependence occurs by the impurity effect at very low temperature around $T \sim 2\eta = 0.02t$. As for the d-wave pairing in Figure 1b, The zero field case shows the T^2-behavior [5,4], which is characteristic of the line node of the $d_{x^2-y^2}$-wave superconductivity. For $H \neq 0$, it is modified to the T-linear dependence [6,8] at low T region.

It is seen in Figure 1 that there exists a crossover temperature T^* both in the s-wave and the d-wave pairing cases, when we consider the dependence of $\kappa_{xx}(T)$ on the magnetic field. At lower temperature $T < T^*$, $\kappa_{xx}(T)$ increases with raising magnetic field. However, at higher temperature $T > T^*$, $\kappa_{xx}(T)$ decreases as a function of H. It is also noteworthy that $\kappa_{xx}(T)$ shows the T-linear behavior at $T < T^*$, while it deviates from T-linear at $T > T^*$. In our parameter, $T^* \sim 0.10t$ in the s-wave case, and $T^* \sim 0.06t$ in the d-wave case.

3.2 Position-resolved thermal conductivity

To understand the abovementioned difference between $T < T^*$ and $T > T^*$, we analyze the position-resolved $\kappa_{xx}(\mathbf{r})$ of equation (30), and investigate how the local thermal flow contributes to the total thermal conductivity. The spatial structures of $\kappa_{xx}(\mathbf{r})$ are shown in Figure 2 for the s-wave pairing and in Figure 3 for the d-wave pairing from low temperature to high temperature. As for the vortex core size, the order parameter recovers at two or three lattice sites from the vortex center at low temperatures. It is seen for both pairing cases that the heat flows

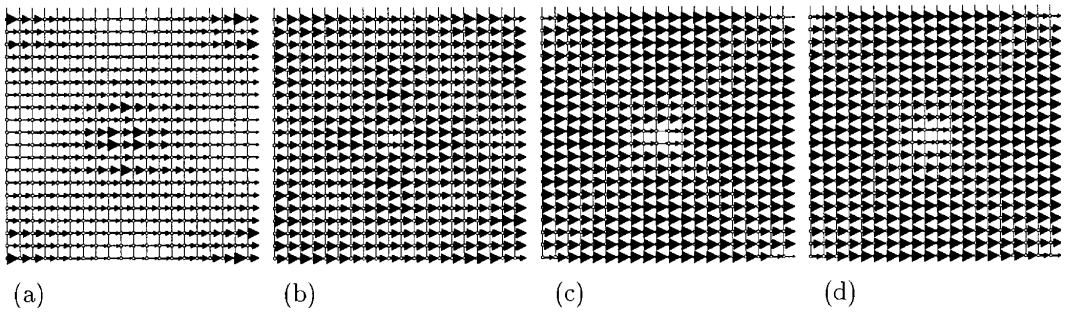

Fig. 3. The vector plots of the $\kappa_{xx}(\mathbf{r})$ in the d-wave pairing case at T/t=0.02 (a), 0.05 (b), 0.09 (c) and 0.13 (d). $H = H_{20}$. The vortices are located at the center and the four corners in the figure. Arrow size is proportional to flow strength.

exclusively at the core region at low T. It comes from the available low energy excitations around the vortex core. Around the core region the heat flow extends to the NN vortex direction. It is due to the inter-vortex quasiparticle transfer effect. With increasing T, the the contributing region of $\kappa_{xx}(\mathbf{r})$ becomes wider around the vortex core and the lines between NN vortices, as seen in Figures 2b and 3b. On the other hand, at higher temperature $T > T^*$, the dominant contribution comes from the outside region of the vortex core. Since $\kappa_{xx}(\mathbf{r})$ is suppressed at the vortex core, the vortex core behaves as if it is a scattering center for the thermal flow. Also along the line connecting NN vortices, $\kappa_{xx}(\mathbf{r})$ is slightly suppressed. At further high T, the heat flows rather uniformly at all region. These higher temperature structure of $\kappa_{xx}(\mathbf{r})$ comes from the contribution of the scattering state at $E > |\Delta|$, as discussed later.

Let us discuss important differences between the s-wave and the d-wave pairing cases. At lower temperature $T = 0.01t$, $\kappa_{xx}(\mathbf{r})$ is well localized at the core region in the s-wave case (Fig. 2a) compared with the d-wave case (Fig. 3a). This difference comes from the line node contribution of the d-wave superconductivity. Due to the line node, the low energy quasiparticle states extend outside of the vortex core, especially to the 45° direction from a and b axis of the crystal lattice [18,20]. At higher temperature $T = 0.09t$, $\kappa_{xx}(\mathbf{r})$ is well suppressed at the core region in d-wave case (Fig. 2c), and it is not too suppressed at the core region in s-wave case (Fig. 3c). To understand these characteristic behavior of $\kappa_{xx}(\mathbf{r})$, we consider the relation between the thermal conductivity and the LDOS.

3.3 Relation with the local density of states

In equation (28), temperature dependence comes from the function $F(E_\alpha, E_\beta)$ in equation (29). It determines which energy level dominantly contributes to the thermal conductivity. To see it, we show the E_α and E_β dependence of $\mathrm{Im}F(E_\alpha, E_\beta)$ in Figure 4. From the figure, we see that $\mathrm{Im}F(E_\alpha, E_\beta)$ becomes large on the line $E_\alpha = E_\beta$. Along the line $E_\alpha = E_\beta = E$, we obtain

$$\mathrm{Im}F(E, E) = E^2 f'(E). \tag{32}$$

Then, $\mathrm{Im}F(E, E)$ vanishes at $E = 0$, and has two peaks at finite energy, which are symmetric with respect to $E = 0$.

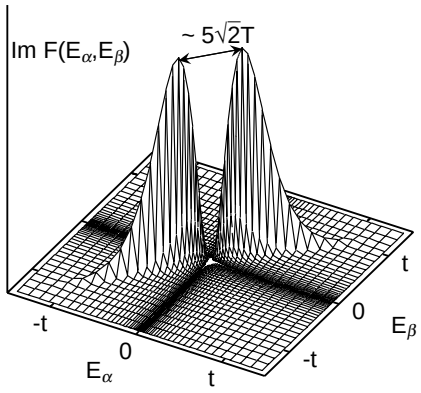

Fig. 4. E_α- and E_β-dependence of the function $\mathrm{Im}F(E_\alpha, E_\beta)$ of equation (29). In this figure, we set η/t=0.01 and T/t=0.10.

The distance of these peaks is about $5\sqrt{2}T$. It means that the quasiparticle states at these peak energy $E \sim \pm 2.5T$ dominantly contributes to $\kappa_{xx}(\mathbf{r})$. At low temperature, the dominant contribution comes from the low energy quasiparticle state around the vortex core. However, at higher temperature, the scattering states at $E > \Delta(T)$ dominantly contribute to the thermal conductivity. In this respect, thermal conductivity is qualitatively different from other physical quantities such as electric conductivity, specific heat [17,19,26], nuclear magnetic relaxation time [27,28]. In these quantities, the quasiparticles at $E \sim 0$ gives largest contribution in all temperature regions. We discuss the electric conductivity at Section 4.

At each energy level E_α, the contribution to the spatial structure of $\kappa_{xx}(\mathbf{r})$ is determined from the spatial distribution of the wave functions $u_\alpha(\mathbf{r})$ and $v_\alpha(\mathbf{r})$. Then, we show the spatial structure of the LDOS at several energies for the s-wave pairing in Figure 5 and for the d-wave pairing in Figure 6. In the s-wave pairing, the low energy quasiparticle states are bound within the vortex core region, and the quantized energy levels appear at half integer energy $E_n = (n + \frac{1}{2})E_\Delta$ [15,16]. Here, E_Δ is the level spacing of the order Δ_0^2/E_F. Δ_0 is the superconducting gap at zero field and E_F is Fermi energy. With the BdG theory at clean limit, since the vortex core radius shrinks to the atomic scale with lowering temperature by the Kramer-Pesch effect [35,36], the quantization effect eminently appears at $T \sim 0$. Then, there are no states just

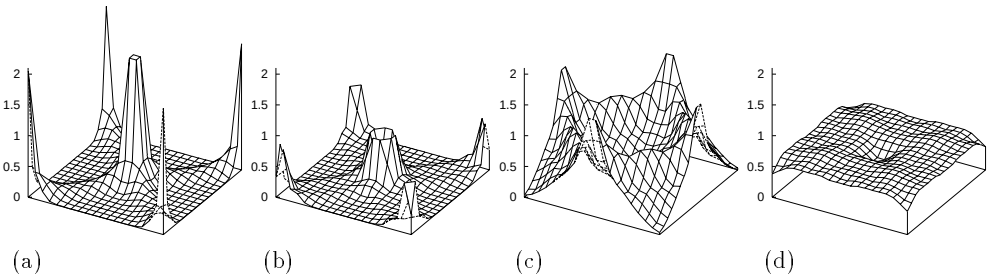

Fig. 5. Local density of states in the s-wave pairing case at E/Δ=0.34 (a), 0.5 (b), 1.0 (c) and 1.5 (d). $H = H_{20}$.

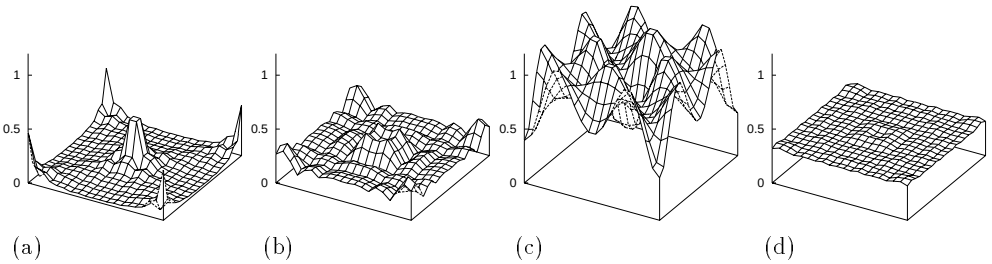

Fig. 6. Local density of states in the d-wave pairing case at E/Δ=0 (a), 0.5 (b), 1.0 (c) and 1.5 (d). $H = H_{20}$.

at $E = 0$ because of the small gap by the quantization in the s-wave pairing. At the lowest energy level $E \sim 0.17t$ in Figure 5a, the LDOS $N(E, \mathbf{r})$ has sharp peak at the vortex center. It is a bound state in the vortex core. At higher energy, the LDOS has peak along a circle around each vortex (Fig. 5b). The radius of the circle increases with raising energy. We also see the small ridge between NN vortices. It is due to the inter-vortex transfer of the low energy bound states. At $E \sim \Delta$, the circle of the LDOS peak around the vortex overlaps each other (Fig. 5c). At higher energy than Δ, the LDOS are reduced to the uniform structure, though the LDOS is slightly suppressed at the vortex core region (Fig. 5d). These energy dependence is consistent with the results of the quasiclassical calculation [37,38].

For the d-wave pairing in Figure 6, since the low energy states extend outside of the vortex core due to the node of the $d_{x^2-y^2}$-wave superconducting gap, energy levels becomes continuous [21,22,26–28]. In Figure 6a, there is a peak of the LDOS at the vortex core at $E = 0$, which corresponds to the zero-bias peak in th spectrum at the vortex center. With increasing E, the peak of the LDOS is shifted to the outside of the vortex, and it is slightly suppressed at the vortex center, as shown in Figure 6b. In the d-wave case, the large LDOS region shows the four-fold symmetric structure instead of the circle structure of the s-wave case. At $E \sim \Delta$, the LDOS peak around the vortex is shifted to the boundary region between vortices (Fig. 6c). At higher energy than Δ, the LDOS are reduced to the uniform structure (Fig. 6d).

3.4 Energy decomposition of thermal conductivity

To discuss the contribution of the LDOS structure to the spatial structure of $\kappa_{xx}(\mathbf{r})$, We decompose $\kappa_{xx}(\mathbf{r})$ of equations (28, 30) into the low energy contribution from $|E_\alpha|, |E_\beta| < \Delta(T)/2$ and the high energy contribution from $|E_\alpha|, |E_\beta| > \Delta(T)/2$. The s-wave pairing case is shown in Figure 7. The upper panels (a) and (b) present the low energy contribution of $\kappa_{xx}(\mathbf{r})$, which are localized around the vortex core and along the line connecting NN vortices. It is because the low energy states for $|E| < \Delta(T)$ are localized around the vortex core and there are some inter-vortex quasiparticle transfer along the NN vortices direction, as shown in Figure 5a and b. The lower panels (c) and (d) show the higher energy contribution of $\kappa_{xx}(\mathbf{r})$ from $|E_\alpha|, |E_\beta| > \Delta(T)/2$. In this energy range, the

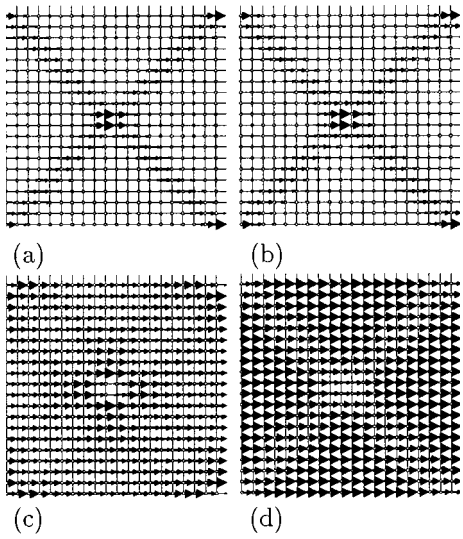

Fig. 7. Energy decomposed $\kappa_{xx}(\mathbf{r})$ in the s-wave case at $T/t = 0.02$ (a,c) and 0.09 (b,d). (a) and (b) are for the low energy contribution from $|E_\alpha|, |E_\beta| < \Delta(T)/2$. (c) and (d) are for the high energy contribution from $|E_\alpha|, |E_\beta| > \Delta(T)/2$.

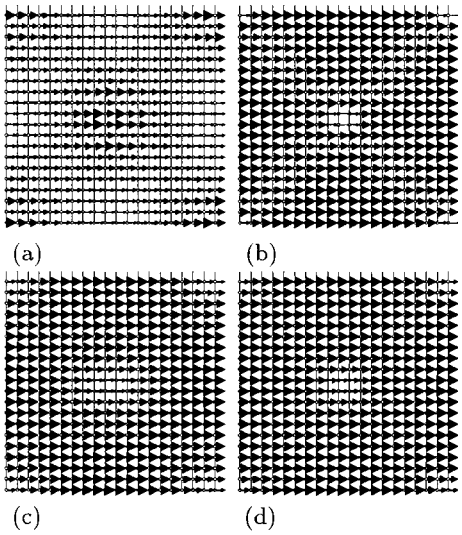

Fig. 8. Energy decomposed $\kappa_{xx}(\mathbf{r})$ in the d-wave pairing case. at $T/t = 0.02$ (a,c) and 0.09 (b,d). (a) and (b) are for the low energy contribution from $|E_\alpha|, |E_\beta| < \Delta(T)/2$. (c) and (d) are for the high energy contribution from $|E_\alpha|, |E_\beta| > \Delta(T)/2$.

wave functions are dominantly located outside of the vortex core, as shown in Figure 5c and d. Then, the higher energy contribution of $\kappa_{xx}(\mathbf{r})$ is suppressed around the vortex core. The suppression along the NN vortices directions shown in Figure 7d also reflects the spatial structure of the LDOS in Figure 5d. At low temperature in Figure 7c, spatial structure is determined by the wave function at $E \sim \Delta(T)/2$ in Figure 5b. However, at high temperature case in Figure 7d, the contribution of the wave function at $E > \Delta(T)$ in Figure 5d is dominant.

The d-wave pairing case is shown in Figure 8. In the upper panels (a) and (b) for the lower energy contribution, $\kappa_{xx}(\mathbf{r})$ is larger around the core and the lines connecting NN vortices. It is broadly extending around the vortex, compared with the s-wave case, because the wave functions are also broadly extending around the vortex core as shown in Figure 6a. At higher temperature, $\kappa_{xx}(\mathbf{r})$ is large outside of the core in Figure 8b, though LDOS at $E = \Delta(T)/2$ are little localized around the core. In the lower panels (c) and (d) for the higher energy contribution, $\kappa_{xx}(\mathbf{r})$ is large outside of the core at every temperature.

Next, we investigate the weight of the energy-decomposed contribution for the spatially averaged κ_{xx}. The temperature dependence is presented in Figure 9. For both pairing cases, we can see that the low (high) energy contribution is dominant at low (high) temperature. The low (high) energy contribution of the d-wave pairing case is larger (smaller) compared with the s-wave pairing case. It is because the d-wave pairing case has larger DOS at $|E| < \Delta(T)$ because the low energy excitation widely extends outside of the vortex core region due to the line node of the superconducting gap. These DOS difference between the d-wave and the s-wave pairing cases is also shown by the quasiclassical calculation (Fig. 18 of Ref. [20]). The very low temperature behavior in Figure 9a in the s-wave pairing at $T < 10^{-2}$ reflects the small gap of the quantized energy level in the s-wave pairing.

4 Electric conductivity

We can also calculate the electric conductivity, if we consider the electric current operator instead of the thermal current operator. Following the same procedure in Section 2.3, the position-resolved electric conductivity is given by

$$\sigma_{xx}(\mathbf{r}_1) = \mathrm{Im}\left\{\frac{\mathrm{d}}{\mathrm{d}\Omega}\frac{1}{N}\sum_{\mathbf{r}_2} Q^{\mathrm{el}}_{xx}(\mathbf{r}_1, \mathbf{r}_2, \mathrm{i}\Omega_n \to \Omega + \mathrm{i}0^+)\right\}\Big|_{\Omega\to 0} \quad (33)$$

with the correlation function

$$\begin{aligned} Q^{\mathrm{el}}_{xx}(\mathbf{r}_1\tau_1, \mathbf{r}_2\tau_2) &= \langle T_\tau[j_x(\mathbf{r}_1\tau_1), j_x(\mathbf{r}_2\tau_2)]\rangle \\ &= T\sum_n e^{-\mathrm{i}\Omega_n(\tau_1-\tau_2)} Q^{\mathrm{el}}_{xx}(\mathbf{r}_1, \mathbf{r}_2, \mathrm{i}\Omega_n) \end{aligned} \quad (34)$$

of the electric current operator

$$\begin{aligned} \mathbf{j}(\mathbf{r}_j, \tau) = &\frac{|e|}{2m}(\mathbf{P}_j + \mathbf{P}^\dagger_{j'}) \\ &\times \sum_\sigma \psi^\dagger_\sigma(\mathbf{r}_{j'}, \tau)\psi_\sigma(\mathbf{r}_j, \tau)|_{j=j'}. \end{aligned} \quad (35)$$

Using the wave functions of the BdG equation, we obtain

$$\begin{aligned} &\frac{\mathrm{d}}{\mathrm{d}\Omega} Q^{\mathrm{el}}_{\mathbf{P}_1\mathbf{P}_2}(\mathbf{r}_1, \mathbf{r}_2, \mathrm{i}\Omega_n \to \Omega + \mathrm{i}0^+)\Big|_{\Omega=0} = \\ &-\frac{|e|^2}{4m^2}\sum_{\alpha\beta} F^{\mathrm{el}}(E_\alpha, E_\beta) \\ &\times \Big[\mathbf{P}_1 u_\alpha(\mathbf{r}_1)u^*_\beta(\mathbf{r}_{1'}) + u_\alpha(\mathbf{r}_1)\mathbf{P}^\dagger_{1'}u^*_\beta(\mathbf{r}_{1'}) \\ &- \mathbf{P}^\dagger_1 v_\alpha(\mathbf{r}_1)v^*_\beta(\mathbf{r}_{1'}) - v_\alpha(\mathbf{r}_1)\mathbf{P}_{1'}v^*_\beta(\mathbf{r}_{1'})\Big] \\ &\times \Big[\mathbf{P}_2 u_\alpha(\mathbf{r}_2)u^*_\beta(\mathbf{r}_{2'}) + u_\alpha(\mathbf{r}_2)\mathbf{P}^\dagger_{2'}u^*_\beta(\mathbf{r}_{2'}) \\ &- \mathbf{P}^\dagger_2 v_\alpha(\mathbf{r}_2)v^*_\beta(\mathbf{r}_{2'}) - v_\alpha(\mathbf{r}_2)\mathbf{P}_{2'}v^*_\beta(\mathbf{r}_{2'})\Big]\Big|_{1=1',2=2'}, \end{aligned} \quad (36)$$

where

$$\begin{aligned} F^{\mathrm{el}}(E_\alpha, E_\beta) = &\int\frac{\mathrm{d}\omega}{2\pi}\int\frac{\mathrm{d}\omega'}{2\pi}\delta_\eta(\omega - E_\alpha)\delta_\eta(\omega' - E_\beta) \\ &\times\left[\mathrm{P}\frac{f(\omega) - f(\omega')}{(\omega-\omega')^2} + \mathrm{i}\pi f'(\omega)\delta(\omega-\omega')\right]. \end{aligned} \quad (37)$$

We show the E_α and E_β dependence of $\mathrm{Im}F^{el}(E_\alpha, E_\beta)$ in Figure 10. The principal value part of equation (37) vanishes by the spatial average of $\sigma_{xx}(\mathbf{r}_1)$. Then, we consider only the contribution of $\mathrm{Im}F^{\mathrm{el}}(E_\alpha, E_\beta)$, neglecting $\mathrm{Re}F^{\mathrm{el}}(E_\alpha, E_\beta)$. The function $\mathrm{Im}F^{\mathrm{el}}(E_\alpha, E_\beta)$ becomes

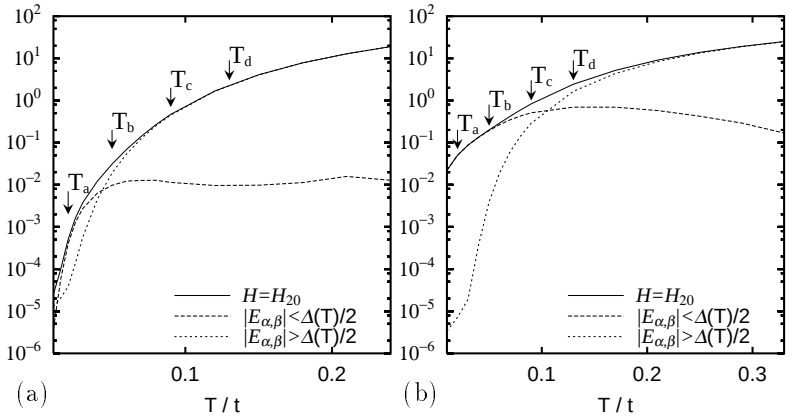

Fig. 9. Temperature dependence of the energy-decomposed κ_{xx}. The low energy contributions from $|E_\alpha|, |E_\beta| < \Delta(T)/2$ and the high energy contributions from $|E_\alpha|, |E_\beta| > \Delta(T)/2$ are shown with the total κ_{xx}(Solid line). $H = H_{20}$. (a) s-wave case. (b) d-wave case. The arrows T_a-T_d show T/t=0.02, 0.05, 0.09 and 0.13, respectively. We show $\kappa_{xx}(\mathbf{r})$ in Figures 2, 3, 7 and 8 at these temperatures.

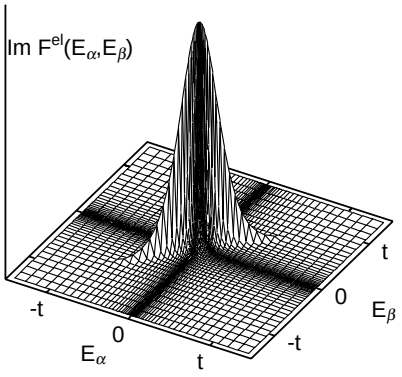

Fig. 10. E_α- and E_β-dependence of the function $\mathrm{Im}F^{\mathrm{el}}(E_\alpha, E_\beta)$ of equation (37). In this figure, we set η/t=0.01 and T/t=0.10.

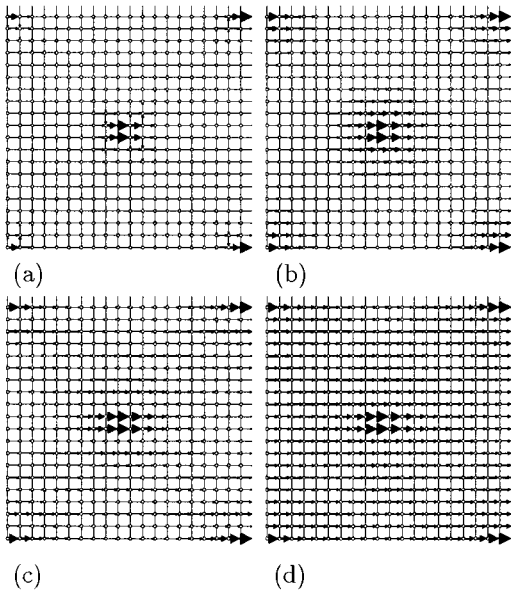

Fig. 11. The vector plots of the position-resolved electric conductivity $\sigma_{xx}(\mathbf{r})$ in the s-wave pairing case at T/t=0.02 (a) and 0.09 (b), and in the d-wave pairing case at T/t=0.02 (c) and 0.09 (d). $H = H_{20}$. The vortices are located at the center and the four corners in the figure. Arrow size is proportional to flow strength.

large for $E_\alpha \sim E_\beta$. Along the line $E_\alpha = E_\beta = E$, we obtain $\mathrm{Im}F^{\mathrm{el}}(E, E) = f'(E)$. It has maximum at $E = 0$ in all temperature region. Then, the low energy quasiparticle states around the vortex core dominantly contribute to $\sigma_{xx}(\mathbf{r})$ even at higher T. We present $\sigma_{xx}(\mathbf{r})$ in Figure 11a, b for the s-wave pairing case and in Figure 11c, d for the d-wave pairing case. Even at higher temperature (b and d), the dominant contribution to σ_{xx} comes from the vortex core region as in the low temperature case (a and c). This is contrasted with the thermal conductivity case, whose dominant contribution comes from the outside of the vortex core at high temperature, as discussed in Section 3. Compared to the s-wave pairing case (a and b), $\sigma_{xx}(\mathbf{r})$ widely extends toward the outside of the vortex core in the d-wave pairing case (c and d). It reflects the extending low energy quasiparticles due to the line node of the d-wave superconducting gap.

5 Summary and discussions

We have formulated thermal conductivity in mixed state based on a microscopic theory of BdG equation and linear response theory. The T-dependence of thermal conductivity κ_{xx} for the s-wave and the d-wave pairing is calculated. Their behaviors are analyzed in terms of the position-resolved thermal conductivity $\kappa_{xx}(\mathbf{r})$. And we discuss the relation between $\kappa_{xx}(\mathbf{r})$ and the LDOS of the quasiparticles around the vortex.

There is a crossover temperature T^*. At lower temperature $T < T^*$, κ_{xx} is increased with raising magnetic field. In these temperature region, thermal flow is dominantly carried by the low energy quasiparticles around the vortex core and their inter-vortex transfer. Then, $\kappa_{xx}(\mathbf{r})$ is large around the vortex core and the lines connecting

NN vortices. On the other hand, at higher temperature $T > T^*$, κ_{xx} is decreased at higher field. In these temperature, the contribution to the thermal conductivity comes from higher energy quasiparticles including the scattering state at $E > \Delta(T)$. Therefore, $\kappa_{xx}(\mathbf{r})$ is suppressed at the vortex core region. Then, vortex core works as if the scattering center for the thermal flow. These contributions from the higher energy states at higher temperature is a characteristic of thermal conductivity. For other quantities such as electric conductivity, specific heat, nuclear magnetic relaxation time, the low energy state gives largest contribution at all temperature regions.

The difference between the s-wave pairing and the d-wave pairing comes from the node structure of the superconducting gap. The d-wave pairing case has larger contribution from the low energy quasiparticle states. The low temperature distribution of $\kappa_{xx}(\mathbf{r})$ is broadly extending around the vortex in the d-wave case, because the wave functions are broadly extending around the vortex core due to the node structure.

Our calculation has reproduced experimental results of the T-linear behavior at low temperature in the vortex states ($H \neq 0$), and the existence of the crossover temperature T^* in the field dependence. The crossover temperature T^* are reported both in the conventional s-wave superconductor such as Nb (Ref. [7]) and in the high-T_c superconductors such as $Bi_2Sr_2CaCu_2O_8$ (Ref. [8]) and in the f-wave superconductor UPt_3 (Ref. [6]). These experimental results have been explained as follows. At low temperature, vortex assist the thermal flow due to the low energy quasiparticle state around the vortex core. At higher temperature, vortex behaves as the scattering center for the thermal flow. Our numerical results of $\kappa_{xx}(\mathbf{r})$ are consistent to this picture. While the field dependence of κ_{xx} is important, our calculation cannot examine the continuous field dependence because we consider the field $H = 2\phi_0/(aN_r)^2$ depending on the size of the unit cell. At higher temperature, there appears the effect of the T-depending η due to the inelastic scattering by antiferro magnetic spin fluctuations [39–41]. For the further extension of our calculation, we will examine the effect of the T-dependence or the position dependence (inside or outside of the vortex core) of the scattering parameter η.

The authors thank N. Hayashi for useful discussions.

References

1. B. Lussier, B. Ellman, L. Taillefer, Phys. Rev. B **53**, 5145 (1996)
2. K. Izawa, H. Takahashi, H. Yamaguchi, Y. Matsuda, M. Suzuki, T. Sasaki, T. Fukase, Y. Yoshida, R. Settai, Y. Onuki, Phys. Rev. Lett. **86**, 2653 (2001)
3. K. Machida, T. Nishira, T. Ohmi, J. Phys. Soc. Jpn **68**, 3364 (1999)
4. P.J. Hirschfeld, W.O. Putikka, Phys. Rev. Lett. **77**, 3969 (1996)
5. S. Schmitt-Rink, K. Miyake, C.M. Varma, Phys. Rev. Lett. **56**, 2575 (1986)
6. H. Suderow, J.P. Brison, A. Huxley, J. Flouquet, J. Low Temp. Phys. **108**, 11 (1997)
7. J.B. Sousa, Physica **55**, 507 (1971)
8. H. Aubin, K. Behnia, S. Ooi, T. Tamegai, Phys. Rev. Lett. **82**, 624 (1999)
9. A. Houghton, K. Maki, Phys. Rev. B **4**, 843 (1971)
10. G.-M. Yin, K. Maki, Phys. Rev. B **47**, 892 (1993)
11. R.M. Cleary, Phys. Rev. **1**, 169 (1970)
12. S. Sergeenkov, M. Ausloos, Phys. Rev. B **52**, 3614 (1995)
13. H. Houssa, M. Ausloos, M. Pekala, Phys. Rev. B **54**, 12713 (1996)
14. S. Dorbolo, M. Ausloos, Phys. Rev. B **64**, 184521 (2001)
15. C. Caroli, P.-G. de Gennes, J. Matricon, Phys. Lett. **9**, 307 (1964)
16. N. Hayashi, T. Isoshima, M. Ichioka, K. Machida, Phys. Rev. Lett. **80**, 2921 (1998)
17. G.E. Volovik, JETP Lett. **58**, 469 (1993)
18. M. Ichioka, N. Hayashi, N. Enomoto, K. Machida, Phys. Rev. B **53**, 15316 (1996)
19. M. Ichioka, A. Hasegawa, K. Machida, Phys. Rev. B **59**, 184 (1999)
20. M. Ichioka, A. Hasegawa, K. Machida, Phys. Rev. B **59**, 8902 (1999)
21. M. Franz, Z. Tešanović, Phys. Rev. Lett. **80**, 4763 (1998)
22. M. Franz, Z. Tešanović, Phys. Rev. Lett. **84**, 554 (2000)
23. C. Kübert, P.J. Hirschfeld, Phys. Rev. Lett. **80**, 4963 (1998)
24. I. Vekhter, A. Houghton, Phys. Rev. Lett. **83**, 4626 (1999)
25. M. Franz, O. Vafek, Phys. Rev. B **64**, 220501 (2001)
26. Y. Wang, A.H. MacDonald, Phys. Rev. B **52**, 3876 (1995)
27. M. Takigawa, M. Ichioka, K. Machida, Phys. Rev. Lett. **83**, 3057 (1999)
28. M. Takigawa, M. Ichioka, K. Machida, J. Phys. Soc. Jpn **69**, 3943 (2000)
29. L.P. Kadanoff, P.C. Martin, Phys. Rev. **124**, 670 (1961)
30. V. Ambegaokar, L. Tewordt, Phys. Rev. **134**, A805 (1964)
31. M. Ichioka, N. Enomoto, K. Machida, J. Phys. Soc. Jpn **66**, 3928 (1997)
32. Y. De Wilde, M. Iavarone, V.I. Metlushko, U. Welp, A.E. Koshelev, I. Aranson, G.W. Crabtree, P.C. Canfield, *Vortex Lattice Structure in $LuNi_2B_2C$*, in *The Superconducting State in Magnetic Fields*, edited by C.A.R. Sá de Melo (World Scientific, Singapore, 1998), Chap. 7
33. V.G. Kogan, P. Miranović, D. M^{c}K. Paul, *Vortex Lattice Transitions*, in *The Superconducting State in Magnetic Fields*, edited by C.A.R. Sá de Melo (World Scientific, Singapore, 1998), Chap. 8
34. H. Won, K. Maki, Phys. Rev. B **53**, 5927 (1996)
35. L. Kramer, W. Pesch, Z. Phys. **269**, 59 (1974)
36. W. Pesch, L. Kramer, J. Low Temp. Phys. **15**, 367 (1974)
37. M. Ichioka, N. Hayashi, K. Machida, Phys. Rev. B **55**, 6565 (1997)
38. M. Ichioka, A. Hasegawa, K. Machida, J. Superconductivity **12**, 571 (1999)
39. R.C. Yu, M.B. Salamon, J.P. Lu, W.C. Lee, Phys. Rev. Lett. **69**, 1431 (1992)
40. P.J. Hirschfeld, D. Vollhardt, P. Wölfle, Solid State Commun. **59**, 111 (1986)
41. M. Matsukawa, K. Iwasaki, K. Noto, T. Sasaki, N. Kobayashi, K. Yoshida, K. Zikihara, M. Ishihara, Cryogenics **37**, 255 (1997)